Unexpected Metal Ion Requirements Specific for Catalysis of the Branching Reaction in a Group II Intron†

Elise Dème, Alexis Nolte, and Alain Jacquier*

Laboratoire du Métabolisme des ARN, CNRS (URA 1300), Département des Biotechnologies, Institut Pasteur, 28 Rue du Dr. Roux, F-75724 Paris Cedex 15, France

Received October 15, 1998; Revised Manuscript Received December 29, 1998

ABSTRACT: The splicing process catalyzed by group II intron ribozymes follows the same two-step pathway as nuclear pre-mRNA splicing. In vivo, the first splicing step of wild-type introns is a transesterification reaction giving rise to a branched lariat intron−3′-exon intermediate characteristic of this splicing mode. In the wild-type introns, the ribozyme core and the substrate intron−exon junctions are carried by the same precursor molecule, making it difficult to distinguish between RNA folding and catalysis under normal splicing reactions. To characterize the catalytic step of the first transesterification reaction, we studied the reversal of this reaction, reverse branching. In this reverse reaction, the excised lariat intron and the substrate 5′-exon can be preincubated and folded separately, allowing the measure of the catalytic rate of the reaction. To measure the catalytic rate of the second splicing step, purified lariat intron−3′-exon intermediate molecules were preincubated and folded prior to the addition of 5′-exon. Conditions could be found where chemistry appeared rate limiting for both catalytic steps. Study of the metal ion requirements under these conditions resulted in the unexpected finding that, for the intron studied, substitution of magnesium ions by manganese ions enhanced the rate of the first transesterification reaction by two orders of magnitude but had virtually no effect on the second transesterification reaction or the 5′ splice site cleavage by hydrolysis. Finally, the catalytic rates measured under optimal conditions for both splicing steps were faster by three orders of magnitude in the branching pathway than in the hydrolytic pathway.

Group II introns are found in bacteria as well as in the organelles of fungi, algae, and plants. They are characterized by a set of RNA secondary structures and tertiary interactions that are conserved despite a high degree of sequence divergence. Several of these introns have been shown to be ribozymes that are able to catalyze their own excision in vitro (for reviews, see refs *1*, *2*). Remarkably, their splicing pathway, which involves two successive transesterification reactions, is identical to the splicing pathway of nuclear pre-mRNA introns. In both systems, the first transesterification reaction is initiated by the nucleophilic attack of the 5′ splice site phosphodiester bond by the 2′-hydroxyl of an internal conserved adenosine located in the distal part of the intron. The resulting 2′−5′ phosphodiester bond and branched lariat form of the excised intron constitute the hallmark of group II and nuclear pre-mRNA splicing (*3*−*6*). While group II introns carry the active site responsible for their own excision, the splicing of nuclear pre-mRNA introns takes place within a very large ribonucleoprotein complex called the spliceosome (*7*). Group II introns are thus useful simplified models to study the catalysis of this type of splicing reaction.

All natural ribozymes require metal ions for efficient activity. Metal ions have at least two distinct functions: they stabilize the structure of ribozymes and they can be directly required for catalysis (for reviews, see refs *8*, *9*). Understanding the role of metal ions in ribozyme catalysis thus requires well-defined experimental systems in which the chemical step can be distinguished from structural rearrangements. Furthermore, it is essential to identify metal ion requirements for each individual reaction step.

Like all other natural ribozymes known to date, except RNase P, group II intron ribozymes are covalently linked (in cis) to their substrates. It follows that, in vivo, transcription, RNA folding, and catalysis are integrated processes that would be difficult to separate kinetically from each other. While it is often feasible in vitro to prevent folding of ribozymes during transcription, separating the folding from the catalytic step has proven to be more difficult. In many cases, this was achieved by splitting ribozymes in at least two structural domains which can be folded independently and added in trans to reconstitute an active ribozyme. In these systems, one of the structural domains carries the substrate and the other remains unmodified by the reaction. This latter piece can thus be considered as a true enzyme. At the saturating concentration of one of the domains, such systems make it possible to measure a catalytic rate constant. However, this catalytic rate constant does not necessarily represent the chemical rate of the reaction. For instance, the ribozyme core may not fold properly in the absence of the

† This work was funded in part by a grant from the French Ministry of Higher Education and Research (ACC-SV5). E.D. was supported by a predoctoral fellowship from the French Ministries of Research and Technology and Higher Education and Research. A.N. was supported by a Long Term Fellowship from the European Molecular Biology Organization.

* To whom correspondence should be addressed. Tel: +33-1-4061 3205. Fax: +33-1-4568 8790. E-mail: jacquier@pasteur.fr.

10.1021/bi982462j CCC: $18.00
Published on Web 02/17/1999

substrate because of an inappropriate choice of the bond along which the two pieces were separated from one another, so that structural steps will affect the catalytic rate constant.

In group II introns, several systems have been described that use this approach to measure a catalytic rate constant (*10*−*14*). The best kinetically characterized system (*10, 11*) monitors the 5′ splice site hydrolysis of an RNA composed of a 5′-exon and intron domains 1−3 upon addition of the highly conserved small domain 5 (*15*). This bimolecular system is thought to represent a reasonable mimic of the first step of splicing by hydrolysis because it proceeds with the same reaction rates as seen for a hydrolytic pathway of splicing under identical reaction conditions (*16*). Moreover, the reaction occurs with the same stereochemical preference as that observed during the first step of cis-splicing by the intron: the introduction of a phosphorothioate in the Rp configuration at the cleavage site prevents 5′ splice site cleavage both by hydrolysis and by transesterification (*17*). Importantly, this reaction has been shown to be most likely limited by the rate of chemistry (*11*), making it a useful model to study the involvement of specific structural intron elements in catalysis (*18*−*20*). However, whether the chemical step of 5′ splice site hydrolysis proceeds with a rate comparable to the chemical rate of the first transesterification reaction is not known because the latter has not yet been determined. In fact, it seems likely that the hydrolytic cleavage reaction does not involve all of the catalytic elements of the ribozyme, and it should be recalled that 5′ splice site cleavage by hydrolysis is not the prevalent way to initiate splicing in vitro, except under peculiar ionic conditions (e.g., high KCl concentrations). In the case of the *Saccharomyces cerevisiae* mitochondrial ai5γ intron (Sc.cox1/5), model precursor transcripts that form structurally homogeneous populations do not use the hydrolytic pathway significantly in absence of KCl (*21*), nor does another kinetically well-behaved group II intron (*22*). Moreover, while the hydrolysis pathway could be detected in vivo with some mutant introns (*23*), it remains very inefficient in these mutants and has never been observed for wild-type group II introns, indicating that branch formation is the prevalent splicing pathway in vivo for this class of introns. Finally, because nuclear pre-mRNA splicing (*3*−*6*) proceeds exclusively by lariat formation, it would seem essential to develop a system that makes it possible to access the catalytic step of the branching reaction of group II introns if these molecules are to be used as substitutes for the spliceosome.

Several bimolecular model systems that perform the branching reaction have been described, but in none of these could conditions be found where chemistry was rate limiting (*13* and F. Michel, personal communication, *14*, *24*). We thought to use another route to gain access to the chemical rate of the first transesterification reaction by studying the reversal of this reaction (reverse branching or debranching). This reverse reaction has been described for some time (*24*−*27*) but is rather inefficient in wild-type introns because the splicing reaction is normally driven forward by a conformational change occurring between the two transesterification reactions (see Figure 1A). This conformational rearrangement, which is mediated by a tertiary interaction (η/η') between domains 2 and 6 (see Figure 1B), can be specifically inhibited by mutations within either of these domains (*28*). These mutations induce the spectacular enhancement of the reverse branching reaction, probably because the first step branch product remains stalled within the active site (*14, 21, 28*). One such mutation, consisting of substitution of the GUAA terminal loop of domain 6 by UUCG, was introduced in the IL/L6 molecule described by Nolte et al. (*21*): incubation of the IL/L6 mutant lariat intron with a short 5′-exon results in the induction of a fast and extensive reverse branching reaction.

Here, we show that conditions can be found under which the chemical step of catalysis is rate limiting. This allowed us to analyze the requirements in divalent cation and monovalent salt concentrations for catalysis of this reaction under conditions where chemistry is rate limiting. We report that at least one metal binding site required for the first transesterification reaction has a much higher affinity for manganese than for magnesium: under conditions usually used to analyze group II intron splicing, nonsaturation of this site by magnesium limits the catalytic rate of this transesterification reaction. Interestingly, addition of manganese does not affect the catalytic rate of 5′ splice site hydrolysis, even under conditions where chemistry is limiting.

We next developed a similar assay, using purified wild-type lariat intron−3′-exon, which reconstitutes a bona fide second splicing step and allows the catalytic rate of the second transesterification reaction to be measured under conditions where chemistry is limiting. Addition of manganese has no or very little effect on the reaction rate under these conditions.

We discuss several hypotheses to explain the specific effect of manganese on the catalytic rate of the first transesterification reaction.

MATERIALS AND METHODS

RNA Synthesis. To obtain sufficient amounts of unlabeled L6 mutant ai5γ lariat intron RNA (IL/L6) for kinetic studies, 500 μg of *Eco*RI digested pSP64/Δ52/L6 plasmid DNA (*28*) was transcribed for 3 h at 40 °C in a 5 mL preparative reaction containing 2500 units of SP6 RNA polymerase (Boehringer), 1 mM NTPs, and 1X transcription buffer (Boehringer). The reaction sample was then treated with 300 units of DNase I for 15 min at 37 °C, extracted with a mixture of phenol/chloroform/isoamyl alcohol (50/45/1; v/v/v; pH 6.7), precipitated with four volumes of 7.5 M (NH_4)-OAc/absolute ethanol (1/6, v/v), rinsed with 70% ethanol, and dried. The RNA pellet was resuspended in 1 mL H_2O, denatured at 95 °C, and cooled slowly to 45 °C. Then, 1 mL of 2X splicing buffer, prewarmed at 45 °C, was added, and this splicing reaction mixture was incubated for 45 min at 45 °C (1X splicing buffer: 100 mM $MgCl_2$, 0.5 M $(NH_4)_2$-SO_4, 40 mM MOPS, pH 7.5). The RNA was desalted using size exclusion chromatography (Microspin S-200 HR columns, Pharmacia), and the lariat intron was purified by preparative 4% polyacrylamide gel electrophoresis (PAGE). After elution from the gel and ethanol precipitation, the RNA was resuspended in 100 μL of water and stored at −20 °C. This yielded 2.75 nmol of lariat intron (as determined by UV-spectrophotoscopy using an extinction coefficient of 40 μg/$OD_{260\ nm}$ unit).

The Rex all-ribose 5′-exon had the following sequence: 5′-CGUGGUGGGACAUUUUC-3′. The Rex-1d 5′-exon had the same sequence but the 3′-terminal nucleotide was a

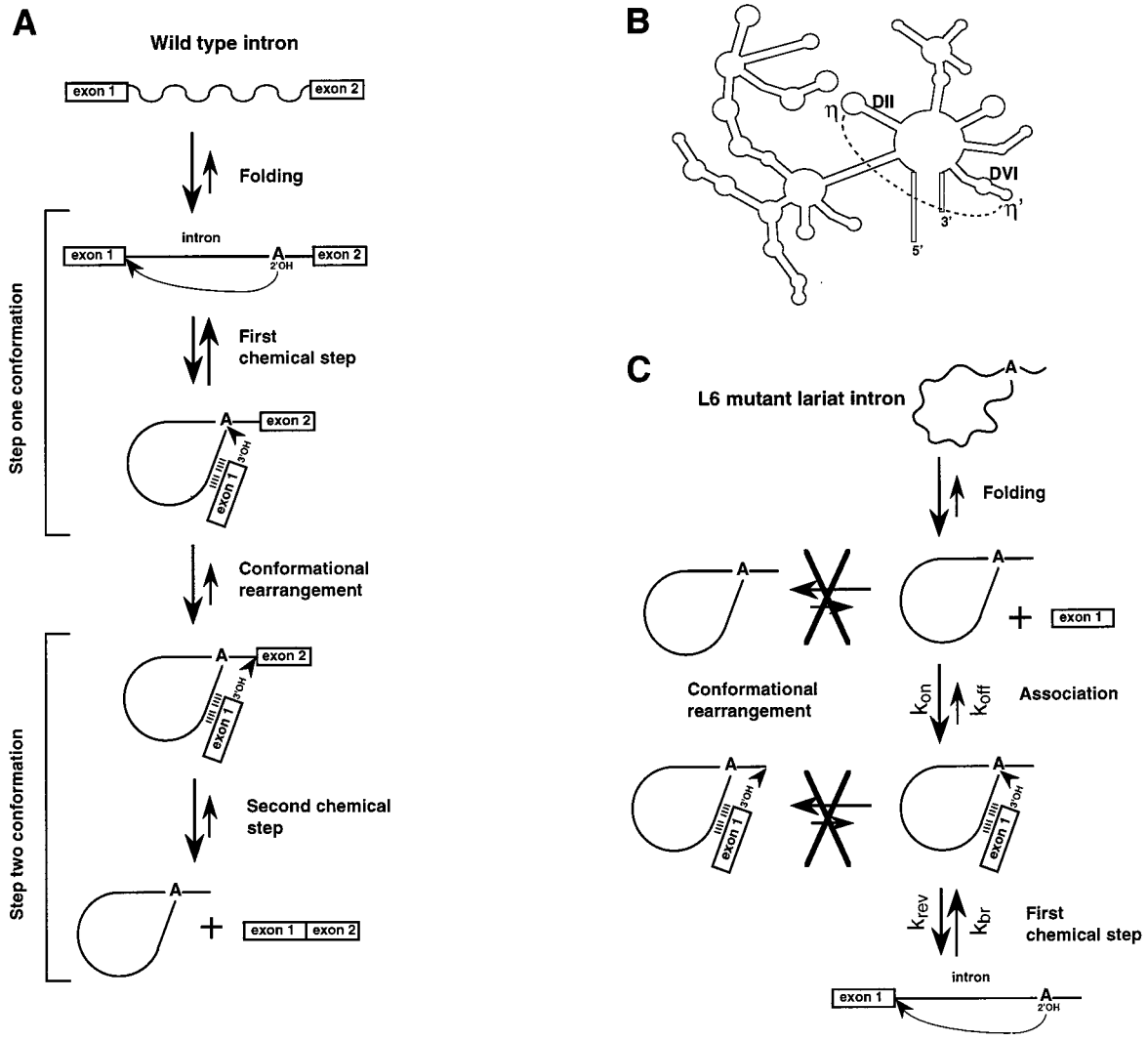

FIGURE 1: Reaction pathways. Intron sequences are represented as continuous lines while exon sequences are represented as boxes. (A) In vitro splicing pathway for the ai5γ group II intron. Arrows represent the different kinetic steps of the reaction that have been identified and also point to the 2′-hydroxyl and 3′-hydroxyl nucleophilic attacks of the 5′ and 3′ splice sites. (B) Simplified schematic representation of the ai5γ group II intron secondary structure. The dashed line points to the η/η' interaction occurring, after the first chemical step, between two GC base pairs within domain 2 (D2) and a GUAA tetraloop capping domain 6 (D6). This interaction is involved in the conformational rearrangement that occurs between the two chemical steps and it stabilizes the step two specific conformation. (C) Reaction pathway of the in vitro reverse branching reaction. The two large black crosses indicate the inhibition of the conformational rearrangement by the L6 mutation (GUAA tetraloop of domain 6 mutated to UUCG) which disrupts the η/η' interaction. In absence of this mutation, the lariat intron would be mainly in the step two specific conformation and would be inefficient for the reverse branching reaction. Here, k_{on} represents the rate of 5′-exon/lariat intron complex formation and k_{off} represents its rate of dissociation. k_{br} and k_{rev} represent the catalytic rates of the branching and reverse branching reactions, respectively.

deoxynucleotide. Both 5′-exons were obtained by chemical oligonucleotide synthesis (Genset, Paris). These 5′-exon oligonucleotides were 5′ end labeled as follows: 10 pmol of oligonucleotide was incubated for 30 min at 37 °C in a 20 μL reaction mix containing 10 pmol of [γ-^{32}P]ATP (ICN, 4500 Ci/mmol), 2 μL 10X kinase buffer (Biolabs), and 10 units of T4 polynucleotide kinase (Biolabs). After labeling, the enzyme was inactivated by heating 10 min at 95 °C and the labeled oligonucleotides were diluted 25 times (20 nM) and used directly for the reverse branching reactions (see below).

Reverse Branching Kinetics. The reverse branching reactions were performed as follows: the 5′ end labeled 5′ exon at 20 nM (5 nM final concentration) and the unlabeled mutant lariat intron IL/L6 at a 4X concentration relative to the final expected concentration in the reverse branching reaction were denatured separately, in water, by incubation for 1 min at 95 °C and slowly cooled to 45 °C in a PCR machine at a rate of 0.2 °C/s between 95 and 55 °C and 0.1 °C/s between 55 and 45 °C. The samples were preincubated for 4 min at 45 °C before the addition of an equal volume of prewarmed 2X splicing buffer (final concentrations: 40 mM MES-NH_4 (pH 5.2−6.5) or MOPS-NH_4 (pH 7.0−7.5), 0.5 or 1.5 M $(NH_4)_2SO_4$ (as specified), and variable $MgCl_2$ and/or $MnCl_2$, concentrations (as specified)). After additional incubation for 6 min at 45 °C, the intron and exon solutions were mixed and aliquots were taken at different times (samples of 0.4 μL were added to 1.6 μL formamide loading buffer at 4 °C). All reactions were performed in a volume of 10 μL, in 500 μL siliconized reaction tubes. Manipulation of the samples and incubation in a 45 °C water bath were performed within an oven heated at 42−45 °C. Moreover, micropipets and

tips were also equilibrated at 42−45 °C. These precautions minimized temperature fluctuations during manipulation and sampling and prevented condensation on the caps of the tubes. Reverse splicing products were separated by 10% PAGE. The gels were fixed for 15 min in a solution consisting of 20% ethanol and 10% acetic acid, then dried, and the reaction products were quantified using a PhosphorImager (Molecular Dynamics). Rate constants were calculated from the fit of the time courses to an equation taking into account the reversibility of the reaction, as described (*21*).

Second-Step Kinetics. To produce the circular intron intermediate, we first transcribed with SP6 RNA polymerase a Δ13-1G variant of intron ai5γ from a mutated pSP64/Δ13 plasmid (*29*). In this mutant, the last nucleotide of the 5′-exon (a C) is replaced by a G. The resulting 5′-exon had the following sequence: 5′-gaauacaagcuugcGUGGGACAUUUUG-3′, where lowercase letters, uppercase letters, and the underlined letter correspond, respectively, to vector-derived sequences, 5′-exon sequences, and the C to G substituted 3′-terminal nucleotide. The crude transcription product was 3′-end labeled with [α-^{32}P]ddATP using the "splint" technique (*30*) as described in Chanfreau and Jacquier (*28*) using the following template deoxyoligonucleotide: 5′-ttttttttttAATTCTTCTAGGCATACCATTAATACC-3′, where upper case letters correspond to the sequence complementary to the 3′-terminal sequence of the precursor RNA. After digestion of template DNA by RNase-free DNase I (Pharmacia), labeled precursor RNA was purified by phenol extraction, exclusion chromatography on Microspin S-200 columns (Pharmacia), and ethanol precipitation. Precursor RNAs were resuspended in water, denatured at 95 °C, slowly cooled to 45 °C, and spliced by incubation in 1X splicing buffer at 45 °C (see above). The circular intermediate was separated from unreacted precursor RNA by 4% PAGE and, after autoradiography, was recovered from gel fragments by overnight elution, phenol extraction, and ethanol precipitation. Second-step kinetics were performed exactly as reverse branching kinetics by co-incubation at 45 °C of the labeled circular intermediate and an excess of the Rex −1d exon RNA (1 μM) in the appropriate splicing buffer (0.5 M ammonium sulfate, 100 mM $MgCl_2$, 40 mM MES at pH 5.2, 5.45 or 6.0). Manganese was always added shortly before initiating the reaction by dilution of a 1 M stock solution to a final concentration of 10 mM. Products, i.e., the ligated exons, were separated by 5% PAGE and quantified with a PhosphorImager. Reaction rates were calculated by exponential fitting of the data plotted as fraction of product versus time.

5′-Hydrolysis Kinetics. The precursor RNA was obtained by SP6 transcription of plasmid pSP64/Δ52 (*29*) linearized by *Hpa*II (which cleaves off domain 6) in the presence of a 10-fold excess of guanosine over GTP. After digestion of the remaining template DNA by RNase-free DNase I, phenol extraction, Microspin S-200 chromatography, and ethanol precipitation, intron precursor RNAs were end labeled with [γ-^{32}P]ATP using T4 polynucleotide kinase as described above and the labeled RNAs were purified by 4% PAGE. The kinetics of hydrolysis of the 5′ junction were measured similarly to 3′ transesterification by incubating the precursor RNA at 45 °C in splicing buffer consisting of 0.5 M KCl, 40 mM MES buffered at the appropriate pH (pH 5.2, 5.45, or 6.0), and 100 mM $MgCl_2$. When required, $MnCl_2$ was added to the buffer at a final concentration of 10 mM. The reaction product, i.e., free 5′-exon, was separated from unreacted precursor RNA by 4% PAGE and quantified using a PhosphorImager. Reaction rates were calculated by exponential fitting of the data plotted as fraction of product versus time.

RESULTS

Accessing the Chemical Rate of the First Transesterification Reaction. Reversal of the first transesterification reaction, reverse branching, appeared as particularly favorable to gain access to the chemical rate of the first transesterification reaction because the excised intron lariat can be preincubated and folded separately from its 5′-exon, the substrate for this bimolecular reaction (Figure 1C). This reaction should thus allow the discrimination between folding and catalysis. Moreover, the presence of an additional 2′−5′ phosphodiester covalent bond within the lariat form of the intron appears to add a strong topological constraint that favors the formation and maintenance of the active structure (*22*, *31*). The study of reverse branching kinetics was facilitated by the use of a mutant lariat intron, the L6 mutant, blocked in the first step specific conformation by the disruption of the η/η' interaction between intron domains 2 and 6 (Figure 1B, C) and which, as a result, catalyzes the reverse branching reaction very efficiently (*21*, *28*).

To separate the folding step from the catalytic step is often not sufficient to warrant that the catalytic rate is indeed rate limited by chemistry. To meet these conditions it can be necessary to slow the chemical reaction itself to make it rate limiting (see, for example, ref *32*). In the Sc.cox1/5 group II intron, the chemical rate of the hydrolytic cleavage at the 5′ splice site was shown to be lowered about 16-fold by substitution of the last ribonucleotide of the 5′-exon by a deoxynucleotide (*33*). We could anticipate the transesterification reaction to be affected by an equivalent or greater factor. Therefore, we used a chemically synthesized 5′-exon composed of the last 17 nucleotides of the exon, thus spanning the intron binding sequences IBS1 and 2 (*29*), and whose last nucleotide was substituted with a deoxynucleotide in order to limit the rate of chemistry (5′-exon here called Rex-1d).

Figure 2A shows a time course of reverse branching performed with trace amounts of [^{32}P] 5′-end labeled Rex-1d 5′-exon (5 nM) and with a large excess of unlabeled L6 mutant lariat intron (500 nM). The reaction can be described by the following scheme:

$$\mathrm{E1} + \mathrm{IL} \underset{k_{\mathrm{off}}}{\overset{k_{\mathrm{on}}}{\rightleftharpoons}} \mathrm{E1/IL} \underset{k_{\mathrm{br}}}{\overset{k_{\mathrm{rev}}}{\rightleftharpoons}} \mathrm{E1{-}Int}$$

where E1 represents the 5′-exon; IL, the lariat intron; E1/IL, the 5′-exon/lariat L6 intron complex; E1−Int, the linear 5′-exon−intron molecule; k_{on} and k_{off}, the rates of complex formation and dissociation, respectively; k_{br}, the catalytic rate of branch formation; and k_{rev}, the catalytic rate of reverse branching. The reaction products separated on gel were quantified with a PhosphorImager. The initial rates of the reaction were calculated for different L6 mutant lariat intron concentrations by linear regression on the logarithm of the fraction of unreacted exon at early time points (Figure 2B).

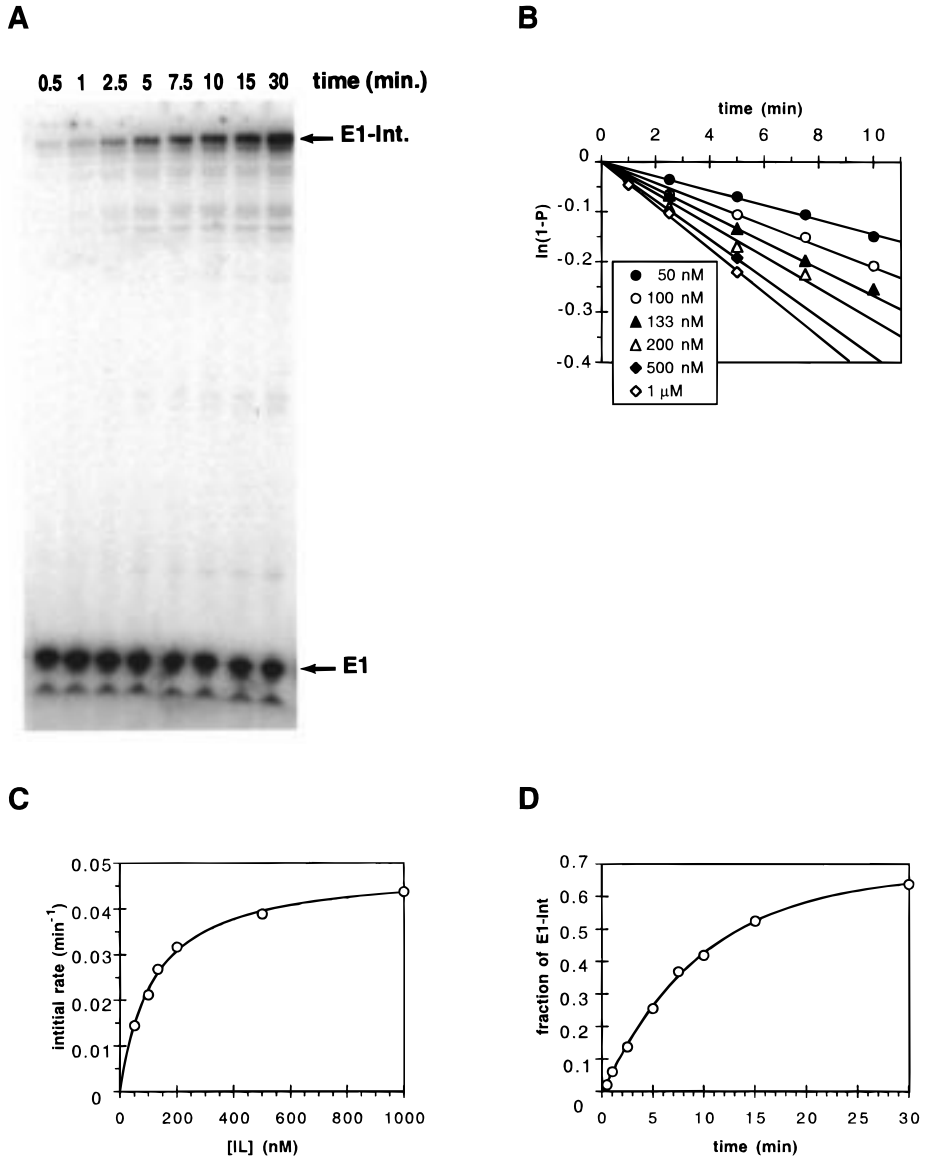

FIGURE 2: The reverse branching reaction exhibits saturation kinetics. (A) Example of a time course for the reverse branching assay. In a typical experiment, 5 nM [^{32}P] 5′-end labeled Rex-1d 5′-exon was incubated with 500 nM unlabeled L6 mutant lariat intron at 45 °C in 0.5 M $(NH_4)_2SO_4$, 100 mM $MgCl_2$, and 40 mM MES-NH_4 pH 6.0 as described in Materials and Methods. Aliquots of the reaction were taken and diluted in ice-cold formamide loading buffer at several time points as indicated. The reaction products were separated by 10% denaturing PAGE and analyzed on a PhosphorImager. The E1 band corresponds to the [^{32}P] 5′ end labeled Rex-1d 5′-exon while the E1-Int band corresponds to the [^{32}P] 5′ end labeled linear 5′-exon−intron molecule, i.e., the product of the reverse branching reaction. (B**)** The plot represents the logarithm of unreacted exons versus time at early time points for increasing concentrations of intron lariat: closed circles, 50 nM, open circles, 100 nM, closed triangles, 133 nM, open triangles, 200 nM, closed diamonds, 500 nM, open diamonds, 1μM. Measures of the initial rates for the reaction were performed by linear regression of these data at early time points. (C) The initial rates measured at early time points for the reverse branching reaction were plotted as a function of the concentration of unlabeled L6 mutant lariat intron ([IL]). The line is the least-squares fit to the Michaelis−Menten equation with $V_{max} = 0.049 \pm 0.002$ min^{-1} and the apparent $K_M = 117 \pm 8$ nM. (D) The fraction of the reverse branching product E1-Int ([E1-Int]/([E1-Int] + [E1])) at each time point was plotted as a function of time. The curve was obtained by fitting the data to a single exponential model equation for reversible reactions at saturating concentrations of lariat intron (see Materials and Methods), allowing the calculation of k_{rev}, the catalytic rate constant for reverse branching.

The plot of the initial rates of the reaction as a function of the concentration of lariat intron, [IL], shows that the reaction follows saturation kinetics (Figure 2C). This plot allowed us to calculate V_{max} and apparent K_M values from a fit of the data to the Michaelis−Menten equation. At saturating concentration of lariat intron ([IL] $\gg K_M$), the rate of formation of the E1/IL complex can be neglected and the reaction reaches a plateau defined as $PL = [E1-Int]_{t\infty}/[IL]_{t0}$ where $[E1-Int]_{t\infty}$ represents the concentration of 5′-exon−intron linear molecules (the product of the reverse-branching reaction) at equilibrium and $[IL]_{t0}$ represents the concentration of lariat L6 intron at time zero. Under these conditions, k_{rev} and k_{br} values can be calculated by plotting the fraction of product ($[E1-Int]_t/[IL]_{t0}$) versus time (Figure 2D) and fitting the data to a simple exponential equation that takes into account the reversibility of the reaction (see Material and Methods).

A hallmark of single-turnover ribozyme reactions limited by the chemical step is that they exhibit a log-linear pH/rate profile with a slope of about 1 (*11*, *34*−*37*). Figure 3 represents the observed rate of reverse branching as a function of pH measured with 5 nM [^{32}P] 5′-end labeled Rex-

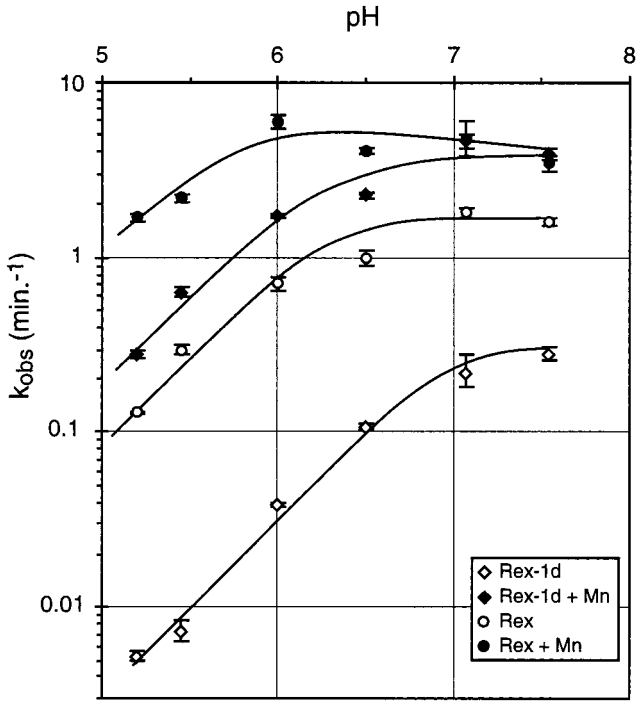

FIGURE 3: Rates of reverse branching plotted as a function of pH. Reactions were performed as described in Materials and Methods, with 500 nM unlabeled L6 mutant lariat intron and 5 nM [^{32}P] 5′ end labeled Rex-1d (diamonds) or Rex (circles) 5′-exons. Reactions were performed in 0.5 M $(NH_4)_2SO_4$, 40 mM of either MES-NH_4 (pH 5.2−6.0) or MOPS−NH_4 (pH 6.5−7.5), 100 mM $MgCl_2$, and with (closed symbols) or without (open symbols) 10 mM $MnCl_2$. The k_{obs} values were shown to be good approximations of k_{cat} at least between pH 5.2 and 6.5 for the all-ribose Rex 5′-exon, between pH 5.2 and 6.5 for the Rex-1d 5′-exon, and between pH 5.2 and 6 for Rex-1d with 10 mM $MnCl_2$ added (see text). Error bars represent the standard errors derived from the fits of the data.

1d 5′-exon and 500 nM unlabeled L6 mutant lariat intron (i.e., a concentration ∼5-fold higher than the apparent K_M measured at pH 6.0; see Figure 2C). The least-squares linear fit of the values between pH 5.2 and 6.5 gave a slope of 1.06 ± 0.08, exactly as expected for a reaction rate limited by chemistry over this entire range of pH. We measured the apparent K_M of the reaction to be ∼139 ± 56 nM at pH 5.2 and ∼110 ± 19 nM at pH 6.5. This indicates that the intron concentration was indeed reasonably saturating in that range of pH over which the pH/rate profile is linear, and shows that our measures of the observed rates of reverse branching reactions approach the catalytic rates in these conditions. Thus, within this range of pH, the catalytic rate exhibits a log-linear pH/rate profile with a slope of ∼1. This is consistent with the catalytic rate being limited by chemistry under these conditions.

To measure the effect of the substitution of the last 5′-exon nucleotide on reactivity, we measured reverse branching kinetics with an all-ribose 5′-exon, called Rex, instead of with the Rex-1d 5′-exon. The pH/rate profile of these reactions is reported in Figure 3 and can be compared to the pH/rate profile obtained with the Rex-1d 5′-exon. The linear least-squares regression of the pH/rate profile gave a slope of 0.96 ± 0.15, between pH 5.2 and 6.0, with a plateau above pH 6.0. This gives a somewhat narrowed linear window compared with the range of linearity from pH 5.2 to almost 7.0 observed with the Rex-1d 5′-exon. Apparent K_M values at pH 5.2 and 6.0 were ∼55 ± 21 nM and ∼139 ± 24 nM, respectively, indicating that the rates measured with 500 nM of lariat intron are reasonable estimates of the catalytic rates, at least over this range of pH. The apparent pK_a observed here may be due in part to the intron being not saturating at higher pH. Significantly, when the rates were compared at pH 6.0, that is within the linear range, the reactions performed with the all-ribose Rex 5′-exon were ∼20-fold faster than the reactions performed with the Rex-1d 5′-exon (in an independent set of experiments, we measured an effect of ∼15-fold; data not shown). Thus, the substitution of the last 5′-exon nucleotide by a deoxynucleotide inhibited the reverse branching reaction by a factor similar to the 16-fold effect on the chemical rate of the hydrolytic cleavage reaction reported earlier (*12*, *33*). The single deoxy substitution appears to similarly affect the catalytic rates of both the reverse branching and the chemically rate limited 5′ splice site hydrolysis, which provides additional strong evidence that the branching reaction is also limited by chemistry under our conditions.

Manganese Addition Dramatically Enhances the Rate of the First Transesterification Reaction. The reactions described above were all performed in the presence of 100 mM magnesium chloride as the unique source of divalent metal ions. With the all-ribose Rex 5′-exon, the addition of 10 mM manganese chloride to the reaction buffer accelerated the reaction 13-fold at pH 5.2 with 500 nM lariat intron (Figure 3). Under these conditions, however, no pH/rate dependence with a slope of 1 could be observed, showing that chemistry was no longer fully rate limiting (Figure 3). This suggested that the actual acceleration of the catalytic rate could possibly be higher than the 13-fold increase observed at the lowest pH. Figure 3 shows that the use of the Rex-1d 5′-exon allowed a linear pH/rate profile between pH 5.2 and 6.0, with a slope ≈ 0.89 ± 0.18 (apparent K_M ≈ 78 ± 25 nM, 117 ± 41, and 250 ± 110 nM at pH 5.2, 5.45, and 6.0, respectively). Within this range of pH, the rate acceleration upon addition of 10 mM $MnCl_2$ was ∼50-fold. This large effect was unexpected. Several factors, such as the size or the pK_a of the hydrated metal ion, may influence activity. Such a great enhancement, however, is particularly surprising considering that it has been obtained by the addition of 10 mM manganese to the 100 mM magnesium ions already present in the reaction buffer. This led us to suspect that the active site contains at least one metal binding site not saturated at 100 mM magnesium and which exhibits a significantly greater affinity for manganese ions than for magnesium ions. Under these conditions the effect of pK_a or other factors would account for only part of the rate enhancement, the remaining enhancement resulting from the better saturation of this site with 10 mM manganese than with 100 mM magnesium.

To test this hypothesis, we first performed a magnesium chloride titration curve (Figure 4) with the Rex-1d 5′-exon at pH 5.45, 0.5 M monovalent ions (ammonium sulfate). Magnesium chloride was still not saturating at a concentration of 150 mM. We could not test higher concentrations because the reactions became irreproducible, probably because of RNA aggregation. Monovalent ions are known to stabilize RNA structures, but performing the reactions in the presence of 1.5 M $(NH_4)_2SO_4$ instead of 0.5 M did not greatly change the titration curves (see Figure 4). When the reactions were performed in the presence of 10 mM manganese chloride,

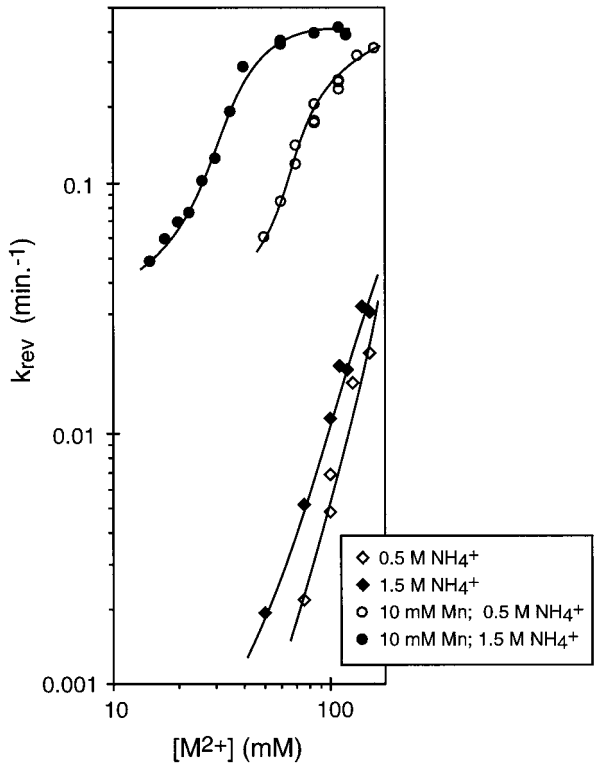

FIGURE 4: Titration of magnesium ions. The rate of the reverse branching reaction is plotted as a function of the concentration in $MgCl_2$. [M^{2+}] represents the concentration in total divalent cations and includes the 10 mM Mn^{2+} when present. The $MgCl_2$ concentration was varied so as to obtain the [M^{2+}] concentration as indicated on the graph. Reactions were performed with 5 nM [^{32}P] 5′ end labeled Rex-1d 5′-exon and 500 nM unlabeled L6 mutant lariat intron, in the presence of 40 mM MES-NH_4 pH 5.45 and either 0.5 M (open symbols) or 1.5 M (closed symbols) $(NH_4)_2SO_4$, with (circles) or without (diamonds) 10 mM $MnCl_2$.

however, the profiles of the titration curves changed dramatically. Magnesium ions could be titrated, and raising the concentration of $(NH_4)_2SO_4$ from 0.5 to 1.5 M greatly shifted the titration curves, with saturation occurring at lower magnesium concentration (apparent K_{Mg} of ~80 mM at 0.5 M $(NH_4)_2SO_4$ and K_{Mg} of ~35 mM at 1.5 M $(NH_4)_2SO_4$). These observations are fully consistent with the starting hypothesis, namely that, in the presence of 10 mM manganese, at least one metal binding site important for the catalytic step is mainly occupied by manganese ions. In the presence of 10 mM manganese, the magnesium titration curves merely represent the structural requirement for metal ions and monovalent ammonium ions are then able to substitute for part of this requirement. In contrast, the magnesium titration curves in the absence of manganese mainly represent the titration at a site involved in the catalytic step and which remains unsaturated at up to 150 mM magnesium. As expected, once the structural requirements have been fulfilled (above ~100 mM divalent metal ions at 0.5 M $(NH_4)_2SO_4$ and above ~40 mM divalent metal ions at 1.5 M $(NH_4)_2SO_4$), the magnesium titration at the active site is no longer affected by the monovalent ion concentration (Figure 4, curves without Mn^{2+}).

An important prediction of this hypothesis is that, under conditions where the general structural requirements are met, manganese titration should reflect occupancy of the active site and should thus (i) not be affected by the ammonium ion concentration and (ii) exhibit a low apparent K_{Mn} when compared to magnesium. Figure 5 presents such titration curves where the overall divalent metal ion concentration was kept constant (150 mM in 0.5 M $(NH_4)_2SO_4$ and 100 mM in 1.5 M $(NH_4)_2SO_4$) in order to fulfill the structural requirements and where the proportion of manganese varied from 0 to 100%. The prediction was perfectly fulfilled, manganese being easily titrated, with an apparent K_{Mn} of ~15 mM independent of the $(NH_4)_2SO_4$ concentration. Moreover, the catalytic rate of the reaction was still pH dependent at both ends of the curves (data not shown), consistent with chemistry remaining rate limiting under these conditions. Note that, for all of the titration curves presented, we verified that lariat intron concentration remained saturating at each extremity of the curve, indicating that the observed rate constants were good estimates of the catalytic rate constants.

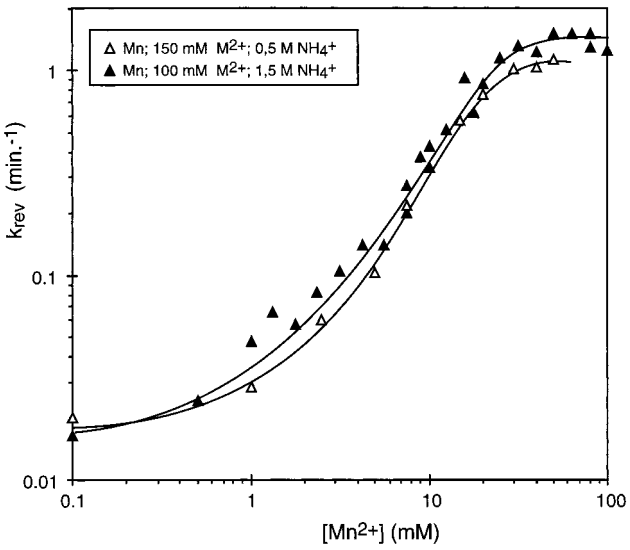

FIGURE 5: Titration of manganese ions. The rate of the reverse branching reaction is plotted as a function of the concentration in manganese ions. Reactions were performed as in Figure 4 except that the total concentration of divalent cations (noted [M^{2+}]) was kept constant in order to fulfill optimal structural requirements: [M^{2+}] = 150 mM in the presence of 0.5 M $(NH_4)_2SO_4$ (open symbols) and [M^{2+}] = 100 mM in the presence of 1.5 M $(NH_4)_2SO_4$ (closed symbols).

Effect of Manganese on the Catalytic Rate of the Second Splicing Step. The important effect of manganese on the rate of the first step transesterification reaction raises the question whether manganese also increases the rate of the second step of splicing. To address this question, we set up a system to measure the rate of the second transesterification reaction under conditions where the reaction is limited by chemistry. In this system the lariat intron−3′-exon intermediate (IL−exon 2) is produced by in vitro transcription of the Δ13-1G ai5γ precursor and subsequent incubation under standard splicing conditions (see Materials and Methods). In this precursor, the 5′-exon lacks part of the intron binding site 2 important for the stability of the 5′-exon/lariat-intermediate complex (*29*). Moreover, substitution of the last C by a G in the 5′-exon introduces a G:G mismatch at the end of the IBS1/EBS1 interaction, further reducing the stability of the intermediate complex. In addition, this substitution dramatically affects the rate of the second splicing step while it has a minor effect on the rate of the first splicing step (A.J.; unpublished observations). It results that this precursor RNA

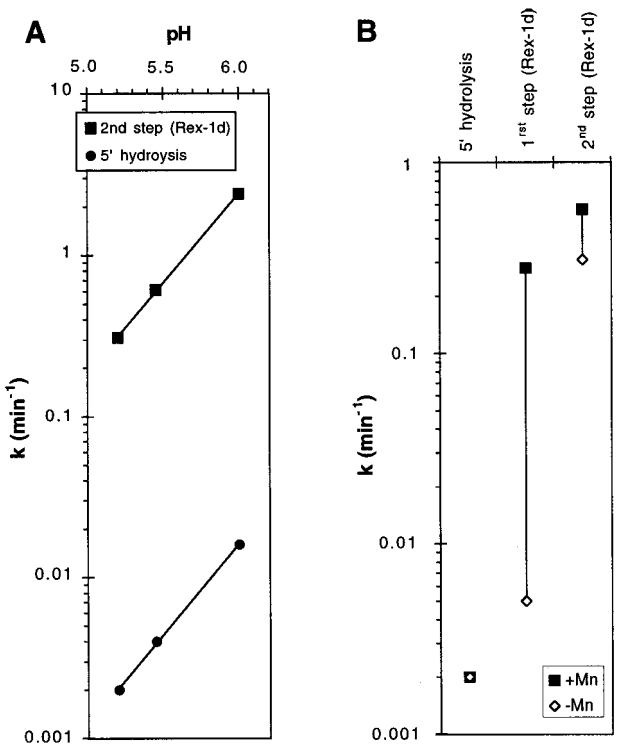

FIGURE 6: (A**)** Rates of second step transesterification (squares) and 5′ splice site hydrolysis (circles) plotted as a function of pH. The rate constants *k* for both reactions were determined as described in Materials and Methods. For both reactions, log (*k*) increases linearly with pH with a slope of ~1.1 for hydrolysis (circles) and a slope of ~1.1 for the second step (squares). The curves suggest that the chemical step is rate limiting for both hydrolysis and second step. Note that the reaction rates for the second step were determined using the Rex-1d exon. (B**)** Effect of manganese on 5′ splice site hydrolysis (noted 5′ hydrolysis), first step and second step transesterification reaction. The figure represents on a logarithmic scale the reaction rates, *k*, in the absence (open diamonds) and in the presence (filled squares) of 10 mM manganese. The reaction rates were measured under conditions where the chemical step is rate limiting (at pH 5.2 and, for the first and second step transesterificaiton reactions, with the Rex-1d 5′-exon). The lines drawn between data points show the important effect of manganese on the first step.

can undergo the first step of splicing quite efficiently. Because the second step is slow and because the intermediate complex is made unstable, virtually all of the molecules that react accumulate in the form of dissociated lariat intron−3′-exon intermediate. Most importantly, because all of the mutations involved are located in the 5′-exon, this mutant precursor RNA allows the production and easy purification of lariat intron−3′-exon molecules with a wild-type sequence.

Starting from the lariat intron−3′-exon intermediate, which was preincubated in the appropriate splicing buffer, the 3′-splicing reaction was initiated by the addition of a 5′-exon containing the IBS1 and IBS2 sequences. When using the all-ribose Rex 5′-exon, this reaction was already very fast at low pH, proceeding at a rate of ~1 min^{-1} at pH 5.2 (data not shown). To achieve conditions under which the chemistry is rate limiting, we measured reaction rates at low pH and we used the modified Rex-1d 5′-exon at saturating concentration (1 μM) to favor exon−intron complex formation (see above). Kinetics were measured at 45 °C in 0.5 M $(NH_4)_2SO_4$ and 100 mM $MgCl_2$ buffered at the appropriate pH with 40 mM MES. Figure 6A displays the effect of pH on the rate of the second step of splicing and shows that the logarithm of the rate of the reaction increases linearly with pH with a slope of ~1.1. Thus, between pH 5.2 and 6.0, this reaction is likely limited by the chemical step. After addition of 10 mM $MnCl_2$ to the reaction buffer at pH 5.2, the reaction rate increases from 0.31 ± 0.05 min^{-1} to 0.57 ± 0.10 min^{-1} (Figure 6B). This corresponds to little, if any, increase in the reaction rate and compares poorly to the 50-fold increase observed for the reverse reaction of the first step of splicing.

Effect of Manganese on Hydrolysis of the 5′-Junction. The above results prompted us to test if the rate enhancement upon addition of manganese could also be observed for the hydrolytic reaction at the 5′ splice site. We therefore measured the reaction rates of 5′-junction hydrolysis under conditions where the reaction is limited by the chemical step (see discussion). For this purpose we synthesized an intron precursor, ai5γ/*Hpa*II, which lacks domain 6 containing the bulged A necessary for branch formation (see Materials and Methods). At 45 °C in 0.5 M KCl and 100 mM $MgCl_2$, this precursor reacted entirely through hydrolysis of the 5′-junction. Figure 6A displays our results and shows that the logarithm of the rate of hydrolysis increases linearly with pH with a slope of ~1.1. According to this plot, the rate of hydrolysis at pH 5.2 is 0.002 min^{-1} and is limited by the rate of the chemical step. Addition of 10 mM $MnCl_2$ to the reaction buffer at pH 5.2 had no effect on the rate of hydrolysis (k_{obs}~0.002 min^{-1}) which contrasts with the results obtained for the first step transesterification (Figure 6B).

DISCUSSION

Reverse Branching is Rate Limited by the Chemical Step at Low pH. Several pieces of evidence substantiate the fact that the reverse branching reaction is limited by the rate of the chemical step below pH 6.0−6.5. First, the catalytic rate increases exponentially with pH, the log(k_{rev}) increasing linearly with pH with a slope of 1. Probably the simplest explanation for this pH dependence is the fact that, during the transesterification reaction, a proton is lost from the 3′-hydroxyl of the attacking nucleotide at the end of the 5′-exon. However, while the log-linear pH dependence of the reaction suggests that its rate is limited by the chemical step, it does not prove it (*36*, *38*). However, another indication that the chemical step is rate limiting under these conditions is the finding that the deoxy substitution of the last 5′-exon nucleotide results in a 15−20-fold decrease of the catalytic rate, a value very close to the 16-fold inhibition of the chemical rate of the 5′ splice site hydrolysis induced by the same substitution (*33*). Also consistent with the reaction being limited by the chemical step rather than by a general structural step is the observation that, when the conditions are optimal for folding, the rate of the reaction is not influenced by the concentration of monovalent ammonium ions in the reaction (see Figure 5).

Estimation of the Forward Branching Rates from the Reverse Branching Reactions. In the present study, we first analyzed the catalytic step of the reverse branching reaction. In fact, this reaction reaches a plateau at equilibrium. If one assumes that most of the RNA population is active, the rate of the forward branching, k_{br}, can be deduced from k_{rev} by using the equation

$$\text{plateau at saturation} = PL = [E1-Int]_{t\infty}/[IL]_{t0} = k_{rev}/(k_{rev} + k_{br})$$

Note that the assumption that most of the RNA is in the active conformation, or is in rapid exchange with it, is supported (but not proven) by the fact that the same kinetic behaviors and the same plateaus are observed if, instead of using traces of labeled 5′-exon and saturating unlabeled lariat intron, one uses traces of labeled lariat intron and saturating unlabeled exon (data not shown). This estimate of k_{br}, however, is more subject to errors than is the measure of k_{rev} because it relies on a good measurement of both k_{rev} and PL. It was especially difficult to precisely measure the PL in conditions where the reactions were slow because it required very extended time courses. Nevertheless, it was striking to see that, when plotting values of k_{br} as a function of pH, the pH/rate profiles obtained were similar to those obtained for k_{rev} (data not shown). The main difference was that the deoxy substitution of the last 5′-exon nucleotide appeared to have a greater effect on branching (about 50-fold) than on reverse branching (20-fold). This was manifested by the fact that the reaction reached an equilibrium of about 0.75−0.80 with the Rex-1d 5′-exon (see Figure 2D) rather than about 0.5 for the all-ribose 5′-exon Rex (see ref *21*). This effect might result from an intrinsic property of the chemical reaction itself or, alternatively, from a structural destabilization of the linear 5′-exon−intron molecule by the deoxy substitution. Further studies will be required to distinguish between these hypotheses. The fact that the pH/rate profiles obtained with the k_{br} values were similar to the profiles obtained with k_{rev} suggests that, under these experimental conditions, the calculated rates of branching are also limited by the chemical step below pH 6.0. It results that the conclusions drawn for the reverse reaction also apply to the forward reaction. In particular, because the addition of manganese had no strong effect on the value of the plateau, it must accelerate equivalently the forward- and reverse-branching reactions. Finally, since the reactions performed with the all-ribose 5′-exon plateau at about 50%, the catalytic rate of branching must be similar to the catalytic rate calculated for reverse branching (see above). This result is in agreement with a previous report (*24*).

In a recent report, the rate of the forward branching reaction was evaluated as a function of pH in a normal forward splicing reaction, taking into account only the fastest reacting population. The authors suggested that factors other than the chemical step contributed to limit the rate of the reaction because the pH/rate profile was complex (*39*). The fact that the pH/rate profile was more complex than in the present study could be due to the fact that it extended to lower pH values: it has been previously suggested that, because there are many groups with p*K*'s of ∼4 in RNA, the slope of the pH/rate profile might be misleading at lower pH values (see *37*). Nevertheless, the rates of the forward branching reactions measured by these authors, under identical conditions (i.e., without manganese), were substantially lower than the rates measured in our system (about 10-fold lower at pH 5.45) suggesting that the chemical step was indeed not fully limiting in the direct analysis of the forward reaction.

The Catalytic Rates of Both Splicing Steps are 1000-fold Faster in the Branching Pathway Than in the Hydrolytic Pathway. Our measures of the catalytic rates of the first step transesterification provide lower limits for the chemical rate of this reaction. It is interesting to compare these values with the chemical rates of the hydrolytic cleavage that have been reported previously. The dependency of the chemical rates of the hydrolytic 5′ splice site cleavage reactions to metal ion concentrations has not yet been analyzed. Hydrolysis was only analyzed in reaction buffers containing 100 mM Mg^{2+}. The measure of the chemical rate of the hydrolytic cleavage was performed in two distinct systems that might differ with respect to their relation to the first or second splicing steps, as suggested from the phosphorothioate stereochemical preferences (*12, 17*). In the first system, the substrate 5′ splice site is in cis of domains 1,2,3, and 5′ splice site hydrolysis is catalyzed by domain 5 provided in trans (*15*). The stereochemical selectivity of this reaction shows that it is related to the first splicing step (*17*). The catalytic rate of this hydrolytic reaction, performed under conditions where the chemical step is rate limiting, at pH 6.0 and with 100 mM Mg^{2+} is ∼0.04−0.1 min^{-1} (*11*). The rate of the reverse branching reaction at pH 6.0 in 100 mM Mg^{2+} and under optimal folding conditions is ∼1 min^{-1}. In the other 5′ splice site hydrolysis reaction (*12*), which is related to the spliced exons reopening reaction (SER) (*12, 17, 40*), the hydrolysis of a small 5′ splice site substrate is catalyzed by a domain 1,2,3/domain 5 complex. The use of a −1 deoxy substrate allows the chemical step to be rate limiting, as estimated by the pH/rate profile (*33*). The rate of hydrolysis of the −1 deoxy substrate at pH 7.5 is 0.17 min^{-1} and at pH 6.0 the rate is ∼0.005 min^{-1}. The rate of the reverse branching reaction under optimal folding conditions and with a −1 deoxy 5′ exon at pH 6.0, in 100 mM Mg^{2+}, but without manganese, is ∼0.04 min^{-1}. Thus, whatever system is used, the transesterification reaction appears faster by about 1 order of magnitude over the hydrolytic cleavage when analyzed with magnesium ions as the only divalent metal ions.

However, if these conditions appear to be optimal for the 5′ splice site hydrolysis reaction, which is not accelerated by the addition of manganese, they do not fulfill the divalent metal ion requirements for the transesterification reaction. Indeed, substitution of part or all of the magnesium ions by manganese ions can accelerate the catalytic rate of the first transesterification reaction up to 100 times. Thus, under optimal conditions, the catalytic rate of the first transesterification reaction is 3 orders of magnitude faster than the rate of the 5′ splice site hydrolysis. The 1000-fold increase in reaction rates for transesterification over hydrolysis shows that the systems that are set up to study hydrolysis are likely to be missing catalytic elements that play a crucial role in the transesterification reaction. These elements would make the 2′-hydroxyl of the branch point, within the structure of group II introns, a much better nucleophile than surrounding water molecules.

Addition of the 5′-exon to a linear form of the intron−3′-exon yeast ai5γ transcript reconstitutes the second step of the hydrolytic splicing pathway (*31, 40, 41*), giving rise to spliced exons and a linear intron. Very recently, it has been shown that, when a 5′-exon with a single 2′ deoxyribose residue at the 3′ end was used in this reaction (−1 deoxy 5′-exon), the catalytic rate was pH dependent, with the log of the rate of the reaction increasing linearly with pH and having a slope of ∼1 (*39*). This suggested that the reaction

was occurring under chemically rate limiting conditions. The observed effects of the Sp phosphorothioate incorporation at the 3′ splice site strengthened this hypothesis. Surprisingly, the rates calculated for this reaction are much slower than our measures of the rates obtained with the lariat form of the same intron−3′-exon intermediate molecule under identical conditions, including the −1 deoxy 5′-exon. At pH 6.0, our measure of the catalytic rate of the second splicing step is ∼2.4 min^{-1} while the reported catalytic rate value for the linear intron−3′-exon is ∼0.003 min^{-1} (*39*). Thus, as for the first splicing step, the hydrolytic pathway results in the second splicing step being, under conditions where the chemical step is limiting, almost 3 orders of magnitude slower than in the normal branching pathway. This is a somewhat unexpected result which suggests that the branch structure is more directly involved at the catalytic step than previously envisioned. A genetically supported interaction has been reported between the branched G1 (the first nucleotide of the intron linked to the branch adenosine by a 2′−5′ phosphodiester bond) and the penultimate nucleotide of the intron (an A) (*42*). This interaction, supported by non-Watson−Crick compensatory base changes, was observed only when the second splicing step occurs with the normal lariat form of the intron−3′-exon intermediate but not with the linear form. An interesting possibility is that this interaction influences the balance of an equilibrium between a structure where the substrate 3′ splice junction is correctly positioned within the active site and a structure where it is incorrectly positioned. In the linear form of the intron, this interaction would not be formed and the equilibrium would be shifted toward the incorrectly positioned 3′ splice site structure. If the equilibrium is rapid, with a relaxation rate faster than the chemical rate of the second transesterification reaction (at least with a −1 deoxy 5′-exon), the reaction would still be rate limited by the chemical step for the linear form of the intermediate (but k_{cat} would be different from k_{chem}). Further studies will be required to test this hypothesis.

Finally, our finding that, in vitro, the chemical steps of both splicing steps can be 1000 time faster in the branching pathway than in the hydrolysis pathway might explain why the branching pathway is a prevalent mode of splicing in vivo.

Metal Ions Are Involved in Catalysis of the Branching Reaction. One of the most surprising results of our study is the large increase of the first transesterification reaction rate upon addition of manganese in conditions where the chemical step is rate limiting. When part of the 100 mM Mg^{2+} ions was substituted by Mn^{2+} ions, the reaction was accelerated up to 100-fold. This unexpected strong enhancement of the catalytic rate observed upon addition of manganese has important implications on the design and the interpretation of experiments aimed at understanding the involvement of metal ions in catalysis by ribozymes. In particular, if the ai5γ group II intron is used as an experimental model, whenever the incorporation of a thiophosphate is thought to directly affect the chemical rate, the interpretation of manganese rescue experiments (*9*) should be done with great caution and should take into account the large general enhancement of the catalytic rate induced by the addition of manganese.

There are a number of possible reasons why a given metal ion might be more effective than another in promoting catalysis by a ribozyme. For example, it has been proposed that the pK_a of the hydrated metal ion, which influences the extent to which it is ionized at a given pH, might partly determine its effectiveness (*34*). Because we could not measure the rate of the reaction at saturation of magnesium ions, we cannot tell if there is a correlation between pK_a and efficiency. However, the fact that substitution of only $^1/_{10}$ of the 100 mM magnesium ions by manganese ions accelerated the catalytic rate 50-fold suggests that manganese was able to displace magnesium very efficiently at one or several sites that are important for the catalytic step. The titration of Mn ions for their effect on catalysis gives an apparent affinity for manganese, K_{Mn}, of less than 15 mM, while magnesium ions are still not saturating at 150 mM (the titration curves suggest that K_{Mg} is at least 10 times higher than K_{Mn}), suggesting that the rate acceleration observed upon addition of manganese results, at least in part, from the greater occupancy of one or several sites by manganese than by magnesium. Several observations support the hypothesis that the manganese titration curve shown in Figure 5 represents the saturation of one or several metal-binding pockets required at the catalytic step but not for general RNA folding. First, the catalytic rate of the reaction remains pH dependent between the two ends of the curve, indicating that the chemical step remains rate limiting throughout the titration curve (data not shown). Moreover, the titration curves are virtually identical whether they are performed at 0.5 or 1.5 M $(NH_4)_2SO_4$. This contrasts with the magnesium titration curves performed in the presence of 10 mM manganese. Under these conditions, saturating concentrations of magnesium can be reached and the titration curves greatly depend on the ammonium sulfate concentration. The latter observation is consistent with the hypothesis that 10 mM manganese fulfills part of the catalytic requirement for the transesterification reaction and that the titration curves in the presence of Mn reflect the metal ion requirement for folding.

Implications of the Catalytic Rate Enhancement Induced by the Addition of Manganese Being Specific to the First Step Transesterification Reaction. The addition of manganese had very little if any effect on the second step of splicing under conditions where the reaction is limited by the chemical step. The acceleration is less than 2-fold, a value which corroborates the 1.3-fold increase published in a recent study (*39*). This contrasts with the large rate enhancement induced by manganese on the rate of the first step transesterification reaction. At first glance, this discrepancy might suggest that the first and second splicing steps are catalyzed within active sites with different metal ion specificities, a conclusion that would disprove a single active site hypothesis, at least in its most simplistic version. This interpretation, however, does not seem to be the most likely one because manganese has no effect on the first splicing step when it occurs by hydrolysis rather than by transesterification. The strong manganese effect is thus specific to the reactions that directly involve the branch site adenosine. Following is a nonexhaustive list of hypotheses that could possibly explain these observations. First, if manganese is directly involved at the chemical step, our findings suggest that it could enhance the reactivity of the 2′ oxygen atom of the branch site: in the forward branching reaction, it would enhance the nucleophilicity of the 2′-hydroxyl; while in the reverse

branching reaction, it would make the 2′ oxygen atom a better leaving group. It would, however, be surprising that the same metal ion could not, in the hydrolytic pathway, influence the reactivity of water molecules as well, except if its binding site is carried by domain 6 itself. Another interesting hypothesis is that there could be a fast equilibrium between a structure in which the 2′ oxygen atom of the branch site (either in the form of an hydroxyl in the forward branching reaction or within the 2′−5′ phosphodiester bond substrate in the reverse reaction) is correctly positioned within the active site and a structure where it is not. If the relaxation time of the equilibrium is faster than the rate of the chemical step, this will not preclude the chemical step from being rate limiting. In this hypothesis, manganese would stabilize the branch site in its correct position and orientation. The structural equilibrium could be very local. For example, the branch site adenosine could be constantly flipping in and out of helix VI (*43*), and the metal ion would displace the equilibrium in one way or another. Effects of this type would not need to involve domain 6 docking. Alternatively, the entire domain 6 could have a low affinity for the active site. Manganese could then stabilize the "docked" state of domain 6. Further studies will be required to distinguish between these hypotheses.

ACKNOWLEDGMENT

We thank G. Chanfreau and F. Michel for critical reading of the manuscript and highly constructive discussions.

REFERENCES

1. Michel, F., Umesono, K., and Ozeki, H. (1989) *Gene 82*, 5−30.
2. Michel, F., and Ferat, J.-L. (1995) *Annu. Rev. Biochem. 64*, 435−461.
3. Padgett, R. A., Konarska, M. M., Grabowski, P. J., Hardy, S. F., and Sharp, P. A. (1984) *Science 225*, 898−903.
4. Ruskin, B., Krainer, A. R., Maniatis, T., and Green, M. R. (1984) *Cell 38*, 317−331.
5. Peebles, C. L., Perlman, P. S., Mecklenburg, K. L., Petrillo, M. L., Tabor, J. H., Jarrell, K. A., and Cheng, H.-L. (1986) *Cell 44*, 213−223.
6. Van der Veen, R., Arnberg, A. C., Van der Horst, G., Bonen, L., Tabak, H. F., and Grivell, L. A. (1986) *Cell 44*, 225−234.
7. Brody, E., and Abelson, J. (1985) *Science 228*, 963−967.
8. Pyle, A. M. (1993) *Science 261*, 709−714.
9. Pan, T., Long, D. M., and Uhlenbeck, O. C. (1993) in *The RNA World* (Gesteland, R., and Atkins, J., Eds.), pp 271−302, Cold Spring Harbor Laboratory Press, Cold Spring Harbor, New York.
10. Franzen, J. S., Zhang, M. C., and Peebles, C. L. (1993) *Nucleic Acids Res 21*, 627−634.
11. Pyle, A. M., and Green, J. B. (1994) *Biochemistry 33*, 2716−2725.
12. Michels, W. J., and Pyle, A. M. (1995) *Biochemistry 34*, 2965−2977.
13. Costa, M., and Michel, F. (1995) *EMBO J. 14*, 1276−1285.
14. Costa, M., Deme, E., Jacquier, A., and Michel, F. (1997) *J. Mol. Biol. 267*, 520−536.
15. Jarrell, K. A., Dietrich, R. C., and Perlman, P. S. (1988) *Mol. Cell. Biol. 8*, 2361−2366.
16. Daniels, D. L., Michels, W. J., Jr., and Pyle, A. M. (1996) *J. Mol. Biol. 256*, 31−49.
17. Podar, M., Perlman, P., and Padgett, R. (1995) *Mol. Cell. Biol. 15*, 4466−4478.
18. Peebles, C. L., Zhang, M., Perlman, P. S., and Franzen, J. S. (1995) *Proc. Natl. Acad. Sci. U.S.A. 92*, 4422−4426.
19. Abramovitz, D. L., Friedman, R. A., and Pyle, A. M. (1996) *Science 271*, 1410−1413.
20. Konforti, B. B., Abramovitz, D. L., Duarte, C. M., Karpeisky, A., Beigelman, L., and Pyle, A. M. (1998) *Mol. Cell 1*, 433−441.
21. Nolte, A., Chanfreau, G., and Jacquier, A. (1998) *RNA 4*, 694−708.
22. Costa, M., Fontaine, J.-M., Loiseaux-de Goër, S., and Michel, F. (1997) *J. Mol. Biol. 274*, 353−364.
23. Podar, M., Chu, V. T., Pyle, A. M., and Perlman, P. S. (1998) *Nature 391*, 915−918.
24. Chin, K., and Pyle, A.-M. (1995) *RNA 1*, 391−406.
25. Augustin, S., Muller, M. W., and Schweyen, R. J. (1990) *Nature 343*, 383−386.
26. Mörl, M., and Schmelzer, C. (1990) *Cell 60*, 629−636.
27. Muller, M. W., Stocker, P., Hetzer, M., and Schweyen, R. J. (1991) *J. Mol. Biol. 222*, 145−154.
28. Chanfreau, G., and Jacquier, A. (1996) *EMBO J. 15*, 3466−3476.
29. Jacquier, A., and Michel, F. (1987) *Cell 50*, 17−29.
30. Hausner, T.-P., Giglio, L. M., and Weiner, A. M. (1990) *Genes Dev. 4*, 2146−2156.
31. Jacquier, A., and Jacquesson-Breuleux, N. (1991) *J. Mol. Biol. 219*, 415−428.
32. Piccirilli, J. A., Vyle, J. S., Caruthers, M. H., and Cech, T. R. (1993) *Nature 361*, 85−88.
33. Griffin, E. A. J., Qin, Z., Michels, W. J., Jr., and Pyle, A. M. (1995) *Chem. Biol. 2*, 761−770.
34. Dahm, S. C., Derrick, W. B., and Uhlenbeck, O. C. (1993) *Biochemistry 32*, 13040−13045.
35. Zaug, A. J., Davila-Aponte, J. A., and Cech, T. R. (1994) *Biochemistry 33*, 14935−14947.
36. Herschlag, D., and Khosla, M. (1994) *Biochemistry 33*, 5291−5297.
37. Knitt, D. S., and Herschlag, D. (1996) *Biochemistry 35*, 1560−1570.
38. Herschlag, D., Eckstein, F., and Cech, T. R. (1993) *Biochemistry 32*, 8312−8321.
39. Podar, M., Perlman, P. S., and Padgett, R. A. (1998) *RNA 4*, 890−900.
40. Jarrell, K. A., Peebles, C. L., Dietrich, R. C., Romiti, S. L., and Perlman, P. S. (1988) *J. Biol. Chem. 263*, 3432−3439.
41. Jacquier, A., and Rosbash, M. (1986) *Science 234*, 1099−1104.
42. Chanfreau, G., and Jacquier, A. (1993) *EMBO J. 12*, 5173−5180.
43. Chu, V. T., Liu, Q. L., Podar, M., Perlman, P. S., and Pyle, A. M. (1998) *RNA 4*, 1186−1202.

BI982462J